

# Study of interdiffusion and growth of topologically closed packed phases in the Co–Nb system

S. S. K. Balam · A. Paul

Received: 24 April 2010/Accepted: 14 August 2010/Published online: 27 August 2010  
© Springer Science+Business Media, LLC 2010

**Abstract** Interdiffusion study of the Co–Nb system is conducted to determine the diffusion parameters in different phases. The integrated diffusion coefficients at different temperatures are calculated for the  $\text{Nb}_2\text{Co}_7$  phase, which has very narrow composition range. The interdiffusion coefficients at different compositions in the  $\text{NbCo}_2$  Laves phase are determined. The interdiffusion coefficient in this phase decreases with increasing Nb content to the stoichiometric composition. Further, the average interdiffusion coefficient in the  $\text{N}_6\text{Co}_7-\mu$  phase is determined. The activation energies for diffusion in different phases are calculated, providing valuable information regarding the diffusion mechanism. In addition, an experiment using Kirkendall markers is conducted to calculate the relative mobilities of the species.

## Introduction

Ni-, Co-, and Fe-based superalloys are extensively used in aircraft engines, land-based gas turbines, rocket engines, and chemical and petrochemical plants because of their excellent corrosion resistance, phase stability, and superior strength at elevated temperatures. Different refractory elements such as Nb, Mo, Ta, W, and Re are added to the alloys to enhance the strength of these materials. However,

during long exposure at high operating temperatures, undesirable topologically closed packed (TCP) phases such as the Laves,  $\sigma$ , and  $\mu$  phases are found to grow. These compounds are very brittle in nature and lead to degradation of the structure [1–3].

The Co–Nb system has drawn special attention because of the presence of different types of Laves phases such as C14, C15, C36 [4], and the  $\mu$  phase. Extensive research is being conducted to develop the Co–Nb phase diagram [4–7]. Stein et al. [4] have recently published a phase diagram that was developed using equilibrated alloys and diffusion couples. This phase diagram is considerably different from the phase diagram proposed by Okamoto [7], which is based on the research by Harikumar et al. [6], especially in the Co-rich alloys.

Some studies on diffusion are available in this system [8–10]. However, further detailed analysis based on a recently reported phase diagram is required [4]. It is necessary to determine the systematic change in the activation energy in the  $\text{NbCo}_2$  Laves phase to understand the diffusion mechanism. The activation energies for the growth of  $\text{Nb}_2\text{Co}_7$  and  $\text{Nb}_6\text{Co}_7-\mu$  should also be determined. Moreover, attempts should also be made to acquire knowledge on relative mobilities of the species.

Therefore, the aim of this study is to investigate interdiffusion in the Co–Nb system. First, the growth kinetics of the phases is determined, and activation energy for growth is calculated. Different diffusion parameters such as interdiffusion, and integrated and average interdiffusion coefficients in the different phases are calculated. The activation energy for diffusion is calculated for all the phases, which reveals the possible diffusion mechanism. Furthermore, experiments on incremental diffusion couples are performed to investigate the relative mobilities of the species.

S. S. K. Balam · A. Paul (✉)  
Department of Materials Engineering, Indian Institute  
of Science, Bangalore 560012, India  
e-mail: aloke@materials.iisc.ernet.in

## Experimental procedure

Diffusion couple technique was used to determine different diffusion parameters. Foils of Co and Nb—having 99.95 wt% purity supplied by Alfa Aesar, USA—were used as starting materials. The foils were cut into pieces of  $6 \times 6 \text{ mm}^2$  cross section and 1-mm thickness. Bonding faces of the couple halves were ground with emery papers and fine polished using 0.25- $\mu\text{m}$  alumina slurry. The polished surfaces were ultrasonically cleaned in ethanol and dried in hot air. Then, the bonding halves were clamped with minimum pressure required in a special fixture to enable good contact. The experiments were performed in vacuum ( $\sim 10^{-6}$  mbar) at temperatures in the range of 900–1200 °C. Once the required vacuum level was achieved, the samples were heated to the target temperature at a rate of 5 °C/min. The temperature was maintained within  $\pm 5$  °C of the target temperature. Before annealing, particles of titanium dioxide ( $\text{TiO}_2$ ) were introduced as Kirkendall markers at the bonding interface. Oxide powder with particle size of about 1  $\mu\text{m}$  was dispersed in acetone and then applied onto the bonding surfaces before joining. In order to investigate the relative mobilities of the species in different phases,  $\text{Nb}_{0.45}\text{Co}_{0.55}$  was melted in an arc melting furnace under an Ar atmosphere and further homogenized for 50 h at 1200 °C to couple it with pure Nb and Co.

After standard metallographic preparation was completed, cross sections of the annealed diffusion couples were examined under a scanning electron microscope (SEM). Composition profiles of the interdiffusion zone were measured using an energy dispersive X-ray spectrometer (EDX) attached to the SEM. Pure Co and Nb were used as standard materials for the measurement. To minimize error in calculations, the stoichiometric composition of the compounds with narrow composition range was used instead of measured composition. The position of the Kirkendall marker plane was located from the presence of X-ray peak of Ti of  $\text{TiO}_2$ .

## Relations used to calculate the diffusion parameters

The parabolic nature of the growth of the phases can be verified by conducting experiments for different annealing times at a particular temperature, and the parabolic growth constant,  $k_p$  of different phases can be calculated from the slope of  $\Delta x^2$  vs.  $2t$ , where  $t$  (s) is the annealing time, and  $\Delta x$  is the layer thickness.  $k_p$  values at different temperatures can then be plotted with respect to the Arrhenius equation to calculate the activation energy,  $Q$  (J/mol) for the growth of the phases.  $k_p$  is given by

$$k_p = k_p^0 \exp\left(-\frac{Q}{RT}\right), \quad (1)$$

where  $k_p^0$  ( $\text{m}^2/\text{s}$ ) is the pre exponential factor,  $R$  (J/mol K) is the gas constant, and  $T$  is the temperature in K.

The interdiffusion coefficient,  $\tilde{D}$  at a particular composition in a binary A–B system can be calculated using the relation proposed by Wagner [11], which is expressed as

$$\tilde{D}(Y^*) = \frac{V_m}{2t} \left( \frac{dx}{dY} \right)^* \left[ (1 - Y^*) \int_{-\infty}^{x^*} \frac{Y}{V_m} dx + Y^* \int_{x^*}^{\infty} \frac{1 - Y}{V_m} dx \right], \quad (2)$$

where  $Y = \frac{N_B - N_B^-}{N_B^+ - N_B^-}$ , and  $N_B$  is the mol fraction of component B in a binary A–B system. The superscripts + and – refer to the mol fraction at un-reacted left ( $x = -\infty$ ) and right-hand ( $x = +\infty$ ) ends of the couple, respectively.  $V_m$  is the molar volume, and  $x$  is the position parameter. “\*” indicates the point of interest.

Furthermore, when the composition of a phase has a very narrow homogeneity range, the slope  $(\frac{dy}{dx})$  cannot be determined because this slope will be almost negligible; Wagner [11] introduced the concept of integrated diffusion coefficient,  $\tilde{D}_{\text{int}}$ , to determine the diffusion parameter.  $\tilde{D}_{\text{int}}$  is the interdiffusion coefficient integrated over the unknown homogeneity range, and for a phase, let us say,  $\beta$  it can be expressed as

$$\tilde{D}_{\text{int}}^\beta = \int_{N_B'}^{N_B''} \tilde{D} dN_B, \quad (3)$$

where  $\Delta N_B^\beta = N_B'' - N_B'$  is the small homogeneity range of the phase.  $\tilde{D}_{\text{int}}$  can be calculated from the composition profile using

$$\begin{aligned} \tilde{D}_{\text{int}}^\beta &= \frac{\left(N_B^\beta - N_B^-\right)\left(N_B^+ - N_B^\beta\right)}{N_B^+ - N_B^-} \frac{\Delta x^2}{2t} \\ &+ \frac{\Delta x}{2t} \left[ \frac{N_B^+ - N_B^\beta}{N_B^+ - N_B^-} \times \int_{-\infty}^{x^{\beta 1}} \frac{V_m^\beta}{V_m} (N_B - N_B^-) dx \right. \\ &\quad \left. + \frac{N_B^\beta - N_B^-}{N_B^+ - N_B^-} \times \int_{x^{\beta 2}}^{\infty} \frac{V_m^\beta}{V_m} (N_B^+ - N_B) dx \right], \end{aligned} \quad (4)$$

where  $N_B^\beta$  is the average composition,  $V_m^\beta$  is the molar volume, and  $\Delta x_\beta$  is the thickness of the  $\beta$  phase.

In some cases, a phase could have reasonable composition range but grows with a very small thickness so that it is difficult to determine the  $(\frac{dy}{dx})$  parameter. In this condition, the integrated diffusion coefficient can first be calculated, and then the average interdiffusion coefficient using

$$\tilde{D}_{av} = \frac{\tilde{D}_{int}}{\Delta N_B}, \quad (5)$$

where,  $\Delta N_B$  is the known composition range of the phase.

The ratio of the intrinsic diffusion coefficient of the species at the Kirkendall marker plane in a phase can be calculated using the relation developed by van Loo [12], which is as follows:

$$\frac{D_{Nb}}{D_{Co}} = \frac{V_{Nb}}{V_{Co}} \left[ \frac{N_{Nb}^+ \int_{-\infty}^{x_K} \frac{Y}{V_m} dx - N_{Nb}^- \int_{x_K}^{\infty} \frac{(1-Y)}{V_m} dx}{-N_{Co}^+ \int_{-\infty}^{x_K} \frac{Y}{V_m} dx + N_{Co}^- \int_{x_K}^{\infty} \frac{(1-Y)}{V_m} dx} \right] \quad (6)$$

where,  $V_{Nb}$  and  $V_{Co}$  are the partial molar volumes of Nb and Co, respectively, at the composition of interest. It is very difficult to determine the partial molar volume of the species in a phase with very narrow homogeneity range. Therefore, it is almost impossible to determine the exact ratio of intrinsic diffusion coefficients in such cases. However, the ratio of intrinsic diffusion coefficient of the species is related to the ratio of tracer diffusion coefficient as follows:

$$\frac{D_{Nb}}{D_{Co}} = \frac{V_{Nb} D_{Nb}^*}{V_{Co} D_{Co}^*} \quad (7)$$

The ratio of tracer diffusion coefficient can be easily calculated using

$$\frac{D_{Nb}^*}{D_{Co}^*} = \left[ \frac{N_{Nb}^+ \int_{-\infty}^{x_K} \frac{Y}{V_m} dx - N_{Nb}^- \int_{x_K}^{\infty} \frac{(1-Y)}{V_m} dx}{-N_{Co}^+ \int_{-\infty}^{x_K} \frac{Y}{V_m} dx + N_{Co}^- \int_{x_K}^{\infty} \frac{(1-Y)}{V_m} dx} \right] \quad (8)$$

Note that we are neglecting the role of vacancy wind effect.

## Results and discussion

Figure 1a shows a scanning electron micrograph of the interdiffusion zone that developed at 1000 °C after annealing for 25 h. Figure 1b shows the corresponding composition profile. Phases developed according to the phase diagram, as shown in Fig. 2, which indicates the presence of  $Nb_2Co_7$ , C15  $NbCo_2$ , and  $Nb_6Co_7-\mu$  phases. On simply looking at the micrograph in Fig. 1a, it seems that only two phases are present. However, composition analysis shows the presence of all the three phases, namely,  $Nb_2Co_7$ ,  $NbCo_2$ , and the  $Nb_6Co_7-\mu$ . Due to the contrast, it is difficult to locate the phase boundary between the  $Nb_2Co_7$  and  $NbCo_2$  phases. Moreover, at higher temperatures (above 1050 °C), it is expected that both the Laves phases (C36 and C15) would grow in the interdiffusion zone. However, the composition difference between the phase boundaries of two  $NbCo_2$  Laves phases is very small and, hence, it is not possible to locate the phase boundaries from the composition analysis. Therefore, we have not reported them as different phases. Furthermore, the

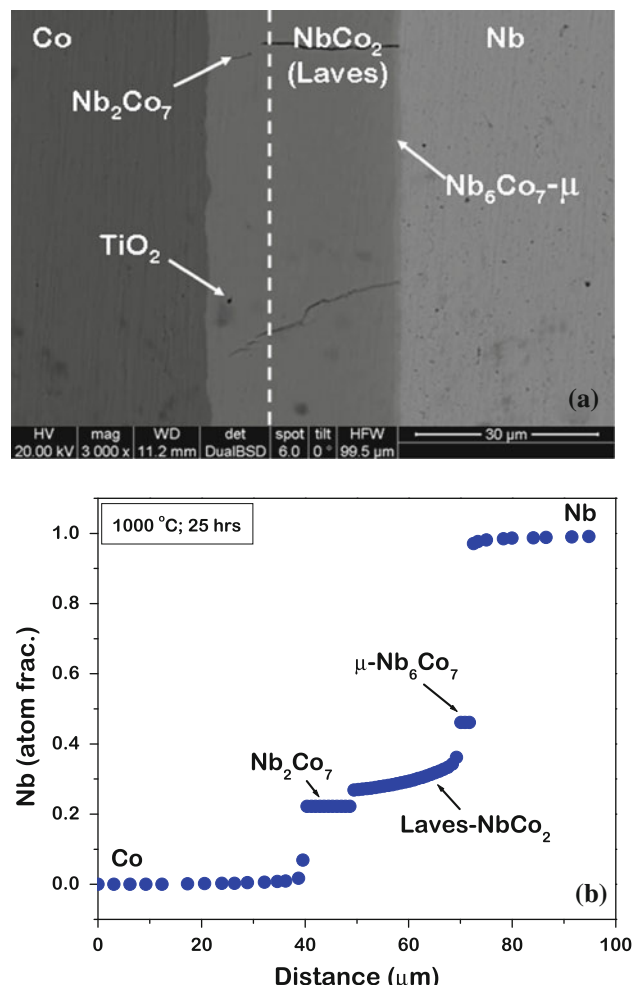


**Fig. 1** **a** Interdiffusion zone of the Co–Nb diffusion couple annealed at 1000 °C for 25 h. White dotted line indicates the position of the  $Nb_2Co_7/NbCo_2$  interphase. **b** Composition profile of the interdiffusion zone

$Nb_6Co_7-\mu$  phase is present in the interdiffusion zone as a thin layer. In order to verify the parabolic nature of the phase growth, interdiffusion was first conducted at 1050 °C for different annealing times. The layer thicknesses of the  $NbCo_2$  Laves phase and the  $\mu$  phase determined at different annealing times are shown in Fig. 3. It was noticed that the data could be fit using the relation  $(\Delta x^2 - \Delta x_o^2) = 2k_p t$ . The positive value of  $\Delta x_o$  indicates that the growth rate of a phase layer is higher at the initial stage. Many times because of small average grain size at the initial stage, higher growth rate is observed due to a large contribution from grain boundary diffusion [12]. Furthermore, the data calculated have been plotted with respect to Eq. 1 and are compared to the data published by Sprengel et al. [8] (Fig. 4). The activation energy for the growth of the  $NbCo_2$  phase was found to be very similar to the results of Sprengel et al. ( $212 \pm 16$  kJ/mol in this study). The activation energy for the growth of the  $Nb_2Co_7$  phase was found to be  $96 \pm 10$  kJ/mol

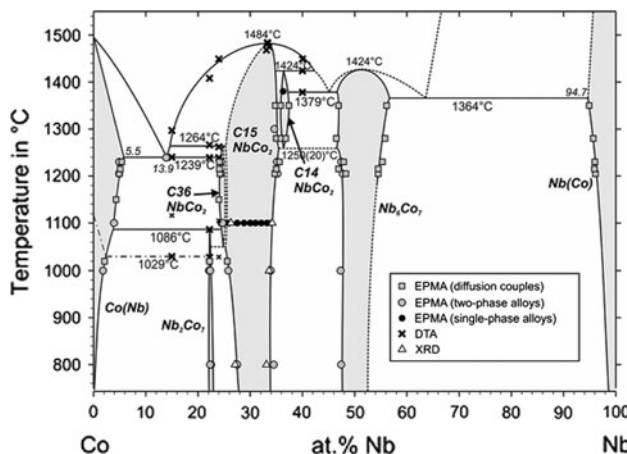


Fig. 2 The Co–Nb phase diagram reported by Stein et al. [4]

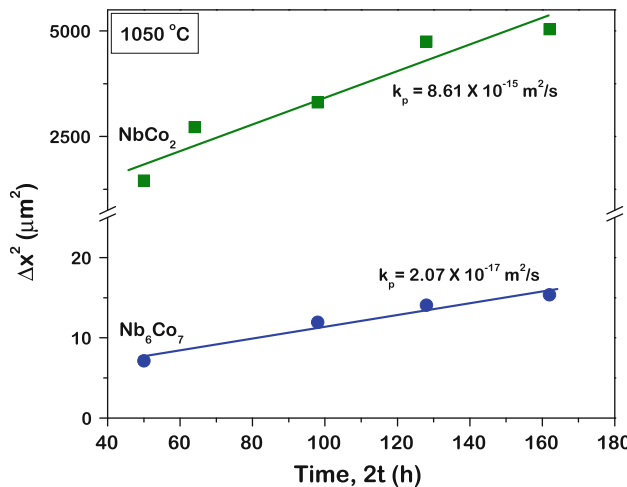


Fig. 3 The parabolic growth of the Laves- $\text{NbCo}_2$  and  $\text{Nb}_6\text{Co}_7$ - $\mu$  phases

in our study against 66.8 kJ/mol in the study by Sprengel et al. Similarly, the activation energy for  $\mu$  phase was found to be  $187 \pm 21$  kJ/mol in our experiment, and data calculated for this phase was not reported by Sprengel et al.

One of the main prerequisites to calculate the diffusion parameters is to know the molar volume of the phases. They have been calculated from the lattice parameter data available in Ref. [4] as follows:  $V_m^{\text{Co}} = 6.7$ ,  $V_m^{\text{Nb}_2\text{Co}_7} = 7.44$ ,  $V_m^{\text{NbCo}_2} = 7.72$ ,  $V_m^{\text{Nb}_6\text{Co}_7} = 8.4$ , and  $V_m^{\text{Nb}} = 10.82 \text{ cm}^3/\text{mol}$ . It should be noted here that the molar volume of the  $\text{NbCo}_2$  phase varies in the range of 7.55–7.89  $\text{cm}^3/\text{mol}$ . We have considered its average value to be 7.72  $\text{cm}^3/\text{mol}$ , which induces just 2% deviation in the molar volume data and becomes insignificant in the calculation of diffusion parameters.

Owing to the nature of the composition profile, it is not possible to determine one type of diffusion parameters for

every phase. The  $\text{Nb}_2\text{Co}_7$  phase grows with a very narrow homogeneity range; therefore, we need to calculate  $\tilde{D}_{\text{int}}^{\text{Nb}_2\text{Co}_7}$  in this phase.  $\tilde{D}_{\text{int}}^{\text{Nb}_2\text{Co}_7}$  calculated at different temperatures using Eq. 4 and plotted with respect to the Arrhenius equation ( $D = D_0 \exp(-\frac{Q}{RT})$ , where  $D$  is the diffusion coefficient, and  $D_0$  is the pre-exponential factor), is shown in Fig. 5. The activation energy calculated for integrated diffusion in this study was  $120 \pm 11$  kJ/mol.

Based on our previous discussion, we can determine  $\tilde{D}$  at different compositions in the  $\text{NbCo}_2$  phase using Eq. 2, and the results are shown in Fig. 6. It can be seen that  $\tilde{D}$  decreases with the increase in Nb content. Since the diffusion of elements is mediated by the defects present in the structure, this trend indicates the possible change in defect concentration of this phase. Furthermore, the average interdiffusion coefficient,  $\tilde{D}_{\text{av}}$  in the  $\mu$  phase was calculated using Eqs. 4 and 5. First, the integrated diffusion coefficient was calculated considering the stoichiometric composition. Then, the average interdiffusion coefficient, as shown in Fig. 5, was determined from the composition range of  $\Delta N = 7$  at.%. The activation energy for  $\tilde{D}_{\text{av}}$  was found to be  $173 \pm 13$  kJ/mol.

As it has already been mentioned that there is no information available on the relative mobilities of the species in  $\text{Nb}_2\text{Co}_7$  and  $\text{Nb}_6\text{Co}_7$  phases, experiments were performed using  $\text{TiO}_2$  particles as Kirkendall markers. In the temperature range of 900–1000 °C, markers were found in the  $\text{Nb}_2\text{Co}_7$  phase. The  $\frac{D_{\text{Nb}}^*}{D_{\text{Co}}^*}$  calculated in this phase was found to be about  $0.05 \pm 0.015$  in the temperature range 900–1000 °C, which indicates that  $D_{\text{Co}}^*$  is about 20 times higher than  $D_{\text{Nb}}^*$ . This is not unexpected considering the Cu<sub>3</sub>Au rule [13], which states that the major element will have a much faster diffusion rate when the ratio of mol fraction of major to minor elements is greater than or equal to three.

As already reported by Stein et al. [4],  $\text{Nb}_2\text{Co}_7$  phase does not form above 1086 °C and mainly two phases ( $\text{NbCo}_2$  and  $\text{Nb}_6\text{Co}_7$ ) grow in the interdiffusion zone. However, in these diffusion couples, we could not locate the position of the markers. In order to gain further information on the relative mobilities of the species in these two phases, experiments on incremental diffusion couples were performed. For example, Fig. 7a shows the incremental diffusion couple  $\text{Nb}_{0.45}\text{Co}_{0.55}/\text{Co}$  annealed at 1150 °C for 25 h. A higher temperature was selected so that only  $\text{NbCo}_2$  phase grew in the interdiffusion zone.  $\text{TiO}_2$  particles used as inert markers were found at the  $\text{NbCo}_2/\text{Co}$  interface, which indicates that Co must have much higher diffusion rate as compared to Nb. Furthermore, since markers were found at the interface, it is not possible to determine the ratio of diffusivities in this phase. However, Denkinger and Mehrer [10] determined the tracer diffusion

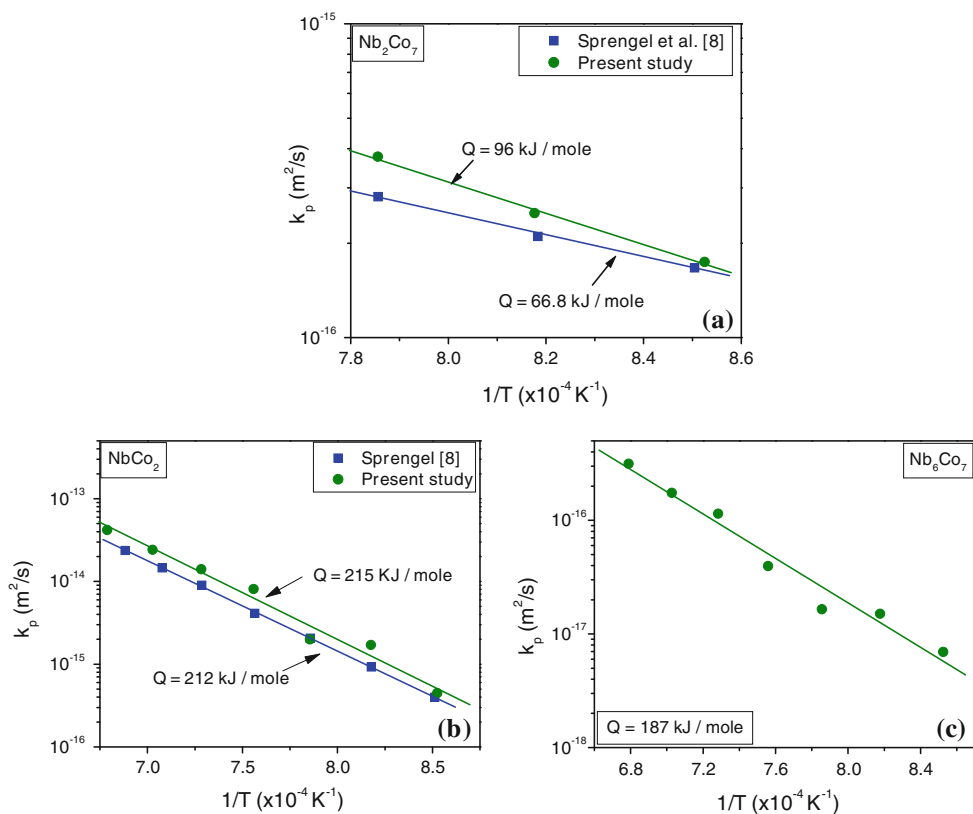


**Fig. 4** The parabolic growth constant of **a**  $\text{Nb}_2\text{Co}_7$ , **b**  $\text{NbCo}_2$  and **c**  $\text{Nb}_6\text{Co}_7$  phases are compared with the data published by Sprengel et al. [8]

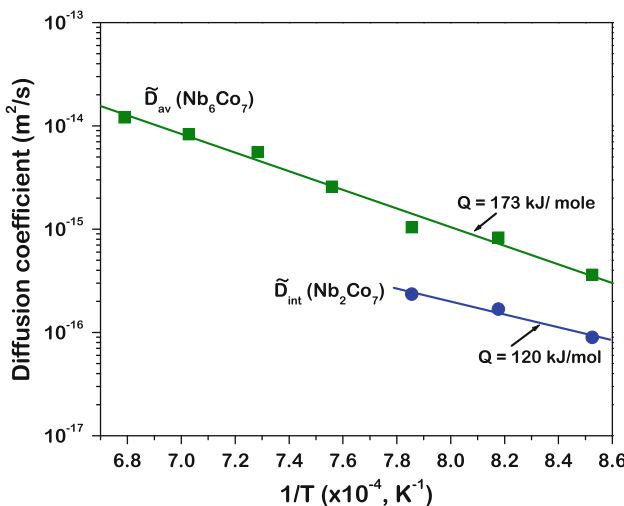


**Fig. 5** The integrated diffusion coefficient of  $\text{Nb}_2\text{Co}_7$  phase and average diffusion coefficient of  $\text{Nb}_6\text{Co}_7-\mu$  phase

coefficient and found that  $D_{\text{Co}}^*$  is two orders of magnitude higher than  $D_{\text{Nb}}^*$  at  $\text{Nb}_{0.31}\text{Co}_{0.69}$ . This validates our experimental results, which indicate that  $D_{\text{Co}}^* \gg D_{\text{Nb}}^*$ .

Furthermore, another incremental diffusion couple  $\text{Nb}_{0.45}\text{Co}_{0.55}/\text{Nb}$  was annealed at  $1150^\circ\text{C}$  for 25 h, as

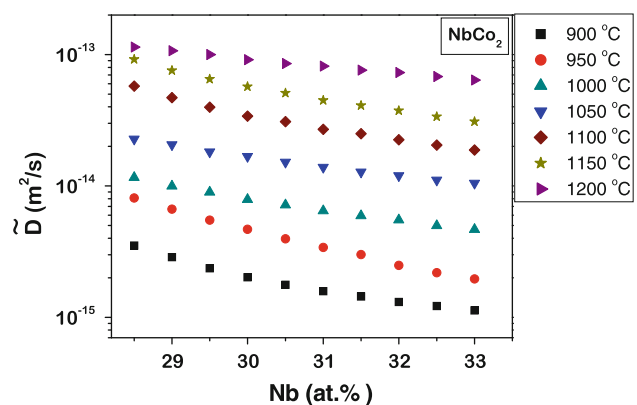


**Fig. 6** The change in interdiffusion coefficients with the change in composition in the  $\text{NbCo}_2$  phase

shown in Fig. 7b, where only the  $\text{Nb}_6\text{Co}_7$  phase grows in the interdiffusion zone. In our analysis, we found that  $\frac{D_{\text{Nb}}^*}{D_{\text{Co}}^*}$  had a negative value. A negative value of  $\frac{D_{\text{Nb}}^*}{D_{\text{Co}}^*}$  is sometimes obtained in the incremental couple because of difficulties in detecting the exact phase boundary. However, this indicates that the value is close to zero, which means that  $D_{\text{Co}}^*$  must be much higher than  $D_{\text{Nb}}^*$  in this phase.

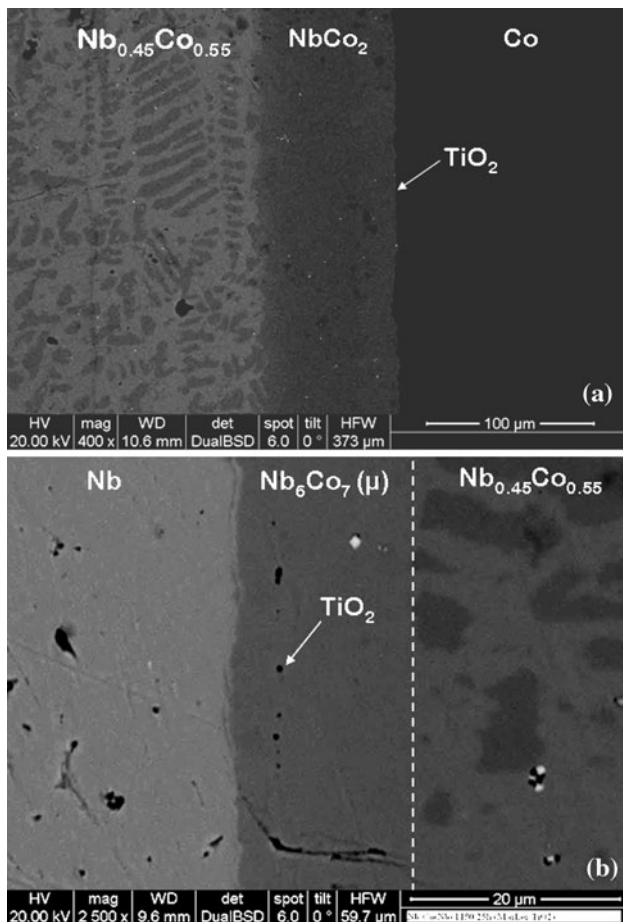


**Fig. 7** **a** The incremental diffusion couple between  $\text{Nb}_{0.45}\text{Co}_{0.55}$  and Co annealed at 1150 °C for 25 h to grow the  $\text{NbCo}_2$  phase is shown. The position of  $\text{TiO}_2$  particle indicates the position of the Kirkendall marker plane. **b** The incremental diffusion couple between  $\text{Nb}_{0.45}\text{Co}_{0.55}$  and Nb annealed at 1150 °C for 25 h to grow the  $\text{Nb}_6\text{Co}_7$  phase is shown. The position of  $\text{TiO}_2$  particle indicates the position of the Kirkendall marker plane. White dotted line indicates the boundary of the interdiffusion zone

## Conclusions

As expected,  $\tilde{D}$  decreases monotonously with the increase in Nb content up to 33 at.% Nb. This is not surprising since the deviation from the stoichiometric composition is compensated by the presence of structural defects, such as antisites, which assist diffusion as seen in the Ni-rich side of the  $\beta$ -NiAl phase [14]. Our analysis on the relative mobilities of the species indicates that Co has much higher diffusion rate as compared to that of Nb. This means that the layer grows mainly because of the diffusion of Co in the interdiffusion zone. Since diffusion rate of Co is very high and that of Nb is negligible, it can be predicted that the presence of Co antisite defects is more dominant than the Nb antisite defects. No data are available for the defect

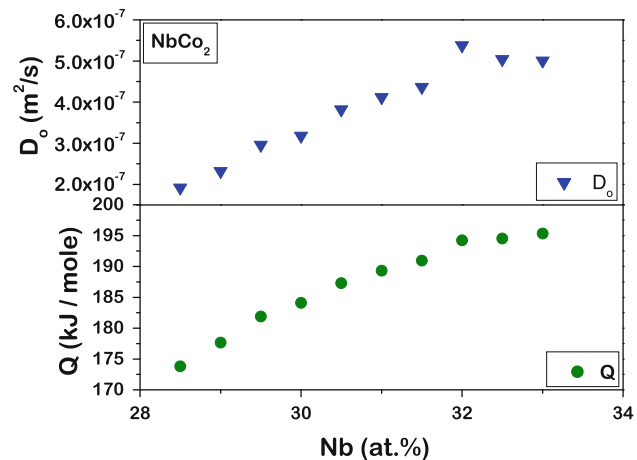


**Fig. 8** The change in pre-exponential factor and the activation energy for interdiffusion coefficient in the  $\text{NbCo}_2$  phase

chemistry in this phase. However, defect concentration data of the  $\text{Co}_2\text{Zr}$  phase having a similar crystal structure is available, and it clearly shows that the concentration of Co antisite defects is much higher compared with Zr, and it increases with the deviation from the stoichiometric composition [15]. Since the defect concentration increases with the deviation from the stoichiometric composition, the activation energy for diffusion should decrease as we deviate from stoichiometry. We find that activation energy certainly decreases with the deviation from stoichiometric composition, as shown in Fig. 8. The activation energy for the integrated diffusion coefficient in the  $\text{Nb}_6\text{Co}_7$  phase was found to be relatively low. In such experiments, we are not able to determine the exact atomic mechanism of diffusion, since we are actually measuring the apparent diffusion coefficient. There could be contribution from both grain and lattice diffusion; however, the low value of activation energy indicates that there must also be a reasonable contribution from grain boundary diffusion in this phase.

## References

1. Yang JX, Zheng Q, Sun XF, Guan HR, Hu ZQ (2007) Mater Sci Eng A 446:100
2. Simonetti M, Caron P (1998) Mater Sci Eng A 254:1
3. Reed RC, Rae CMF (2001) Acta Mater 49:4113
4. Stein F, Jiang D, Palm M, Sauthoff G, Gruner D, Kreiner G (2008) Intermetallics 16:785
5. Pargeter JK, Hume-Rothery W (1967) J Less Common Met 12:366
6. Hari Kumar KC, Ansara I, Wollants P, Delaey L (1998) J Alloys Compd 267:105
7. Okamoto H (2000) J Phase Equilib 21:495
8. Sprengel W, Denkinger M, Mehrer H (1994) Intermetallics 2:127
9. Sprengel W, Denkinger M, Mehrer H (1994) Intermetallics 2:137

10. Denkinger M, Mehrer H (2000) Phil Mag A 80(5):1245
11. Wagner C (1969) Acta Metall 17:99
12. van Loo FJJ (1990) Prog Solid State Chem 20:47
13. d'Heurle FM, Gas PJ (1986) Mater Res 1:205
14. Paul A, Kodentsov AA, Van Loo FJJ (2005) J Alloy Compd 403:147
15. Krčmar M, Fu CL (2003) Phys Rev B 68:134110